SEMI-ANNUAL STATUS REPORT

TO

NATIONAL AERONAUTICS AND SPACE ADMINISTRATION

FROM

THE UNIVERSITY OF TEXAS AT DALLAS
P.O. BOX 688
RICHARDSON, TEXAS 75080
(214) 690-2851

ON

"A RESEARCH IN SUPPORT OF NASA'S SPACE SCIENCE"

NASA Grant NGL 44-004-130
(UTD Account E1306)

For the Period

1 October 1980 - 31 March 1981

W. B. Hanson
Principal Investigator

May 1981

TABLE OF CONTENTS

omit

INTRODUCTION

This report describes the progress and in some cases the final products of the research supported by this grant over the last six months. We have continued to maintain our broad scientific base at UTD and several publications have resulted from our efforts this year. The studies described here have provided new insights into future space flight instrumentation as well as to possible development of new instrumentation stimulated by our theoretical work.

This grant ensures that UTD will continue to respond to the needs of the United States space program and to make invaluable contributions to its productivity beyond that supported on a project basis.

OMIT

SATELLITE INSTRUMENT DIFFICULTIES

A. Spacecraft Contamination

W.B. Hanson

During this grant period we have undertaken an extensive study of contaminent ions observed on the Atmosphere Explorer satellites. Our first objective was to describe the characteristics of the contaminant ions that are liberated from the spacecraft surfaces by the impact of neutral particles and perhaps the ambient ions. The following paper describes these characteristics in more detail and has been submitted for publication in the Journal of Geophysical Research: "Ion Sputtering from Satellite Surfaces."

OMIT

B. Spacecraft Plasma Interactions

The existence of two meter irregularities in the ion flux observed by the RPA's on Atmosphere Explorer C and D have been investigated with the goal of deciding whether they were a natural or spacecraft induced phenomena. A number of possibilities arise if they are in fact a product of a spacecraft plasma interaction and these have been explored theoretically. The following paper describes the characteristics of the observed irregularities and the development of theoretical arguments for a spacecraft plasma interaction. It has been submitted to the Journal of Geophysical Research: "The Case of the Noisy Derivatives - Evidence for a Spacecraft-Plasma Interaction."

D1

STRATOSPHERIC ION COMPOSITION

J.H. Hoffman

A balloon program designed to measure both positively and negatively charged ion species in the stratosphere has been initiated. An instrument design has been created that consists of two identical magnetic sector-field mass spectrometers, one to measure positive species and the other to measure negative species.

The instrument package consists of a hermetically sealed gondola containing the mass spectrometers, cryopumps, ion pumps, electronics, telemeter and instrument battery pack as shown schematically in Figure 1. The flight support package consisting of the tracking beacon, command receiver, battery and parachute and balloon are attached to the gondola via a long lanyard and interconnected by a cable that passes through a hermetic connector in the gondola. A support ring and crash protector upon which the entire flight package may rest is attached to the center flange of the gondola.

Each mass spectrometer consists of an entrance aperture, differentially cryopumped antechamber and entrance chamber, entrance slit, mass analyzer tube, ion pump and electron multiplier detector as shown in Figure 2. Each of these and their functions are described below.

Located at the bottom of the gondola are two entrance apertures each consisting of a small hole (0.5 mm dia.) and sealed by a pyrotechnic opening device which can be operated by command when the balloon reaches cruising altitude. Ambient gases and ions enter through each aperture into the first of two antechambers. As shown schematically in Figure 2 the antechambers are formed by using a thin stainless steel membrane to divide a spherical chamber into two hemispheres. Each of the two antechambers is attached via a chevron baffle to a cryopump. Gases entering the first antechamber are pumped at a sufficient speed to reduce the pressure by 5 orders of magnitude in that volume.

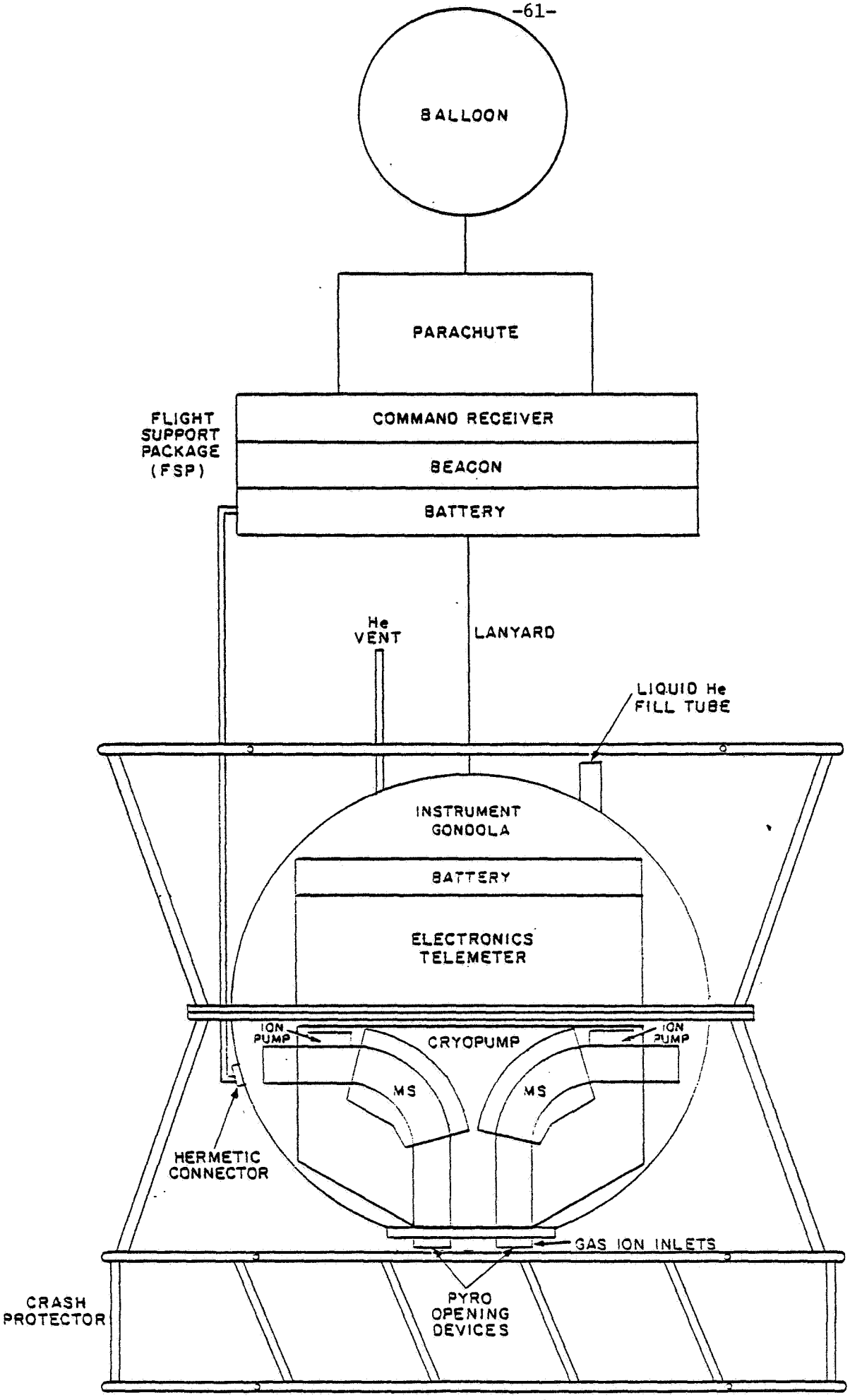
BALLOON
PARACHUTE
FLIGHT SUPPORT PACKAGE (FSP)
COMMAND RECEIVER
BEACON
BATTERY
He VENT
LANYARD
LIQUID He FILL TUBE
INSTRUMENT GONDOLA
BATTERY
ELECTRONICS TELEMETER
ION PUMP
CRYOPUMP
ION PUMP
MS
MS
HERMETIC CONNECTOR
GAS ION INLETS
CRASH PROTECTOR
PYRO OPENING DEVICES

Figure 1.

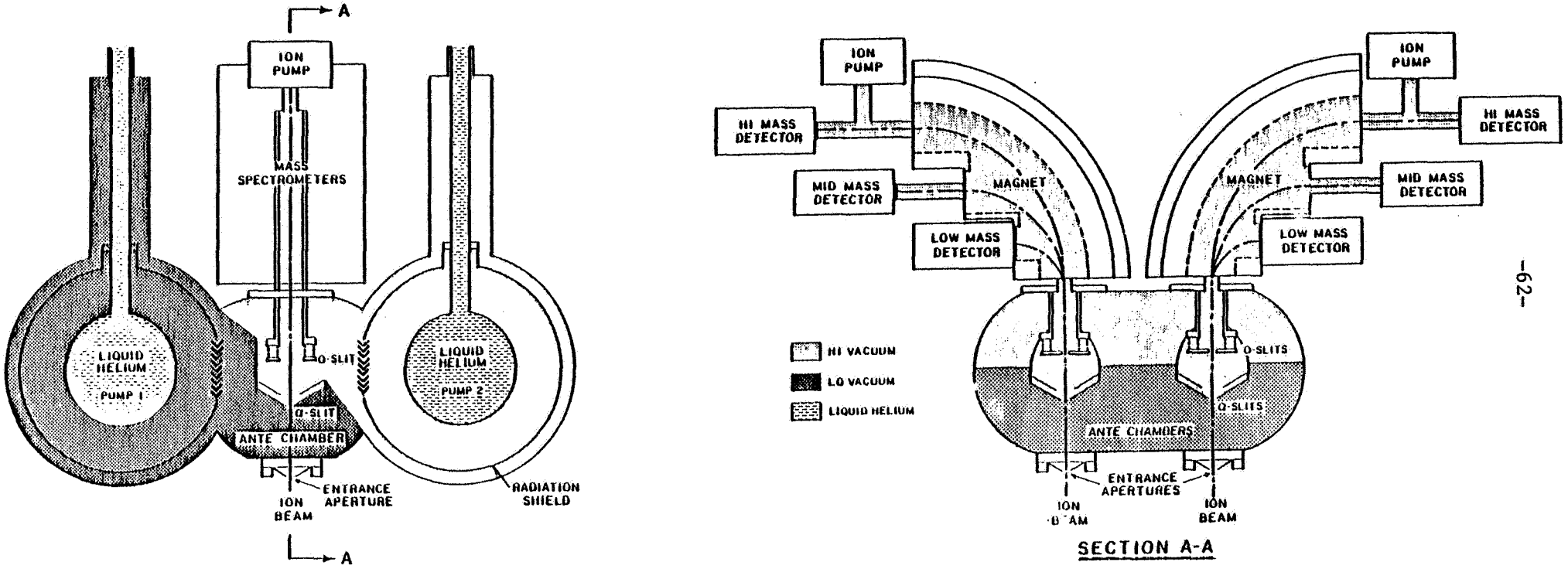
A
ION PUMP
MASS SPECTROMETERS
LIQUID HELIUM
PUMP 1
Q-SLIT
Q-SLIT
ANTE CHAMBER
ION BEAM
ENTRANCE APERTURE
LIQUID HELIUM
PUMP 2
RADIATION SHIELD
A
ION PUMP
HI MASS DETECTOR
MID MASS DETECTOR
LOW MASS DETECTOR
MAGNET
ION PUMP
HI MASS DETECTOR
MID MASS DETECTOR
LOW MASS DETECTOR
MAGNET
HI VACUUM
LO VACUUM
LIQUID HELIUM
Q-SLITS
Q-SLITS
ANTE CHAMBERS
ENTRANCE APERTURES
ION BEAM
ION BEAM
SECTION A-A

Figure 2

Aligned with each of the entrance apertures and located in the membrane itself are two slits (denoted by α in Figure 2). Effluents (neutral and ionic) from the first antechamber pass through the slits and form a beam in the second antechamber. The cryo-pump attached to the second chamber allows a reduction of the pressure in that volume by a factor of 10^4. In addition, the mass analyzer of each mass spectrometer is pumped by an ion pump which also serves as a pressure monitor for the system.

The entrance to each mass spectrometer consists of a single accelerating electrode containing the ion optics object slit (0 in Fig. 2) aligned with one of the α-slits and entrance apertures. Each object slit and subsequent analyzer tube are operated at the potential necessary for transmission of the ion beam through the mass spectrometer. There is no electron emission device, such as a filament, as found in a neutral mass spectrometer because this instrument is designed to only measure ambient ions. After passing through the α-slit, the ions are accelerated through the object slit and into a single focusing magnetic sector field analyzer. The object slit potential is varied from approximately 200 to 830V depending on the mass of the ion to be detected. This potential is negative in the spectrometer that will detect positive ions, and positive in the negative ion analyzer.

Each magnetic mass analyzer has three output channels that cover the mass ranges 12-48, 40-160 and 150-600 amu with a mass resolution (10% valley between adjacent peaks of equal amplitude) of 60 on the low mass channel, 150 on the mid mass channel and 500 on the high mass channel. Mass peak identification out to 600 amu will be possible. Sensitivity is adequate to detect 1 ion/cm^3 with a nominal accumulation period of 1 sec. Using longer periods or integrating a number of periods will improve the sensitivity since background counting rates are typically a few counts per minute.

A microprocessor will control the operation of the instrument. Peak-to-peak stepping, rather than the usual mass scanning will be employed. Initially, five points per mass peak will be measured in a broad search mode to determine the mass numbers of both positive and negative ions and ion clusters. At a 1 second integration per point, it will require 38 minutes to cover the mass range from 12-600 amu.

By way of comparison with instruments flown previously in the stratosphere (Arnold and Fabian, 1980, Arnold, 1980) the instrument proposed for this study has the capability of measuring both positively and negatively charged species in the mass range to 600 amu (a factor of 2 increase) with a resolution of ± 1 amu (an improvement of a factor of 3). These unique features of both extended mass range and high mass resolution will enhance our ability to identify the highly clustered ion species expected in the stratosphere.

In conjunction with the fabrication and integration of the flight package it is necessary to develop laboratory expertise in the preparation, sampling and manipulation of useful fluxes of large cluster ions for pre-flight calibration purposes and postflight analysis of the recorded mass spectra. Based on previous experience it appears that through a judicious choice of pressure and gas composition, it will be possible to produce clustered ion species in afterglow plasmas with masses to approximately 150 amu. For larger clusters it will be necessary to cool the ion source environment itself. Special attention will be directed towards extracting the highly clustered and fragile species of interest and collimating same into directed fluxes useful for calibration of the instrument.

Measured Branching Ratios for O II ^2D and ^2P Transitions In the Wavelength Range 530 to 800 Å

D. MORRISON

University of Texas at Dallas, Richardson, Texas 75080

A. B. CHRISTENSEN

The Aerospace Corporation, El Segundo, California 90009

A. J. CUNNINGHAM

University of Texas at Dallas, Richardson, Texas 75080

Branching ratios for four sets of extreme ultraviolet transitions terminating on the $^2D^0$ and $^2p^0$ metastable levels of ionized oxygen have been measured. The emissions were excited in both an open window hollow cathode and a capillary discharge lamp, and the branching ratios were derived from the observed intensity ratios of the multiplet pairs. The results are in good agreement with theoretical values and compare favorably, within experimental uncertainties, with line ratios obtained by EUV spectroscopy of the airglow.

INTRODUCTION

Recent in situ rocket measurements of the extreme ultraviolet airglow [*Christensen*, 1976; *Gentieu et al.*, 1979] have shown a rich spectrum of neutral and ionic emission lines of atomic O and N lying in the wavelength region 530 to 1200 Å. Amongst the prominent observed O II dayglow transitions (identified by the heavy lines in Figure 1) several are seen to terminate on the $^2D^0$ and $^2P^0$ metastable states of the ion and thereby constitute a production channel for these aeronomically important, long-lived, and reactive species.

To facilitate interpretation of the observed emission spectra in terms of contributing atomic processes, reliable independent information concerning the oscillator strengths and branching ratios of the relevant transitions is required. For the O II transitions highlighted in Figure 1, only calculated values for these parameters are presently available, and the differences between the entries shown in Table 1 can be directly correlated with the calculational scheme adopted. For example the majority of the values summarized in the National Bureau of Standards tables [*Weise et al.*, 1966] were obtained by *Kelly* [1964] using a self-consistent field calculation. However, configuration mixing effects, which were neglected in this approach, are expected to be important for $2s^22p^3$–$2s2p^4$ transitions. The values reported by *Cohen and Dalgarno* [1964] shown in Table 1 were obtained using an expansion method that included the effects of degenerate configurations.

In the work reported here, the EUV spectra from a windowless discharge lamp has been analyzed to allow determination of the branching ratios of the 4 pairs of multiplets listed in Table 1. The transitions studied originate from the lowest lying ^2D and ^2P atomic levels and terminate in the metastable levels. Several quartet transitions terminating on the ground state of the ion were also studied. For convenience in this text each multiplet will be identified by its listed wavelength.

EXPERIMENT DESCRIPTION

A schematic overview of the experimental geometry used in this work is shown in Figure 2. A windowless discharge lamp was connected via a differentially pumped section to a ½-m McPherson Seya-Namioka monochromator. For exciting O^+ transitions either a hollow cathode lamp [*Paresce et al.*, 1971] or a McPherson capillary discharge lamp was used. The latter design was found to deliver larger EUV fluxes. Using a 600-*l*/mm grating, a first-order resolution of 0.5 Å throughout the 500-Å to 1500-Å wavelength interval could be realized. Both a magnetic electron multiplier and a CsI overcoated spiraltron electron multiplier operated in the saturated pulse counting mode were used to detect the dispersed radiation. Output pulses were fed via a frequency meter and a rate meter to either a strip chart recorder or to an acquisition system based on an Apple II minicomputer for permanent storage and subsequent analysis.

Discharges in pure O_2 were struck at source pressure between 40 and 150 μ Hg and at currents between 100 and 500 ma. The principal neutral and ionic emission features excited in the wavelength region 500–840 Å are identified in the spectrogram reproduced in Figure 3. Most of the lines are doublet transitions terminating in the $^2P^0$ and $^2D^0$ metastable states of the ion.

The relative intensity of the multiplets was determined by integrating over the multiplet profile. For those transitions originating on the ^2D levels, the separation of the multiplet components is known to be less than ~0.1 Å, which is too narrow to be resolved by our equipment; however, for the ^2P transitions the separation of the components is 0.5–0.8 Å, so that some structure was evident.

The only significant overlapping of spectral features occurs for the O II (538) and O II (539) multiplets. The spectrum is shown in Figure 4. The weak O II (538) is seen to be just resolved next to the adjacent bright ($^4S^0$–^4P) multiplet.

The data were reduced to give the ratio of the multiplet intensities defined as $r = I(^2D)/I(^2P)$. Since the transitions terminating on the ^2D level were most intense, this ratio was greater than unity. Multiplet intensities were corrected for the wavelength dependence of the detector efficiency and the grating efficiency.

Ratios measured at the various pressures using the two discharge sources are collected in Table 2. No significant pressure dependence was found for doublet transitions terminating on the metastable levels. This was also true for the O II (539) multiplet but not for the strong O II(834) transition. Both these latter transitions terminate on the ground state of the ion, but any resonance scattering problems would be expected to show up first for the O II(834). Its oscillator strength is about a factor of 4 larger than that for O II(539). [*Wiese et al.*, 1966]. The absence of any pronounced pressure dependence of the $^2D^0$ and $^2P^0$ ratios argues against any bias introduced by multiple scattering effects.

The possible influence of absorption by background O and O_2 in the lamp on the ratio measurements was examined as follows. Table 3 lists the total absorption cross section for the multiplets in O_2, N_2, and O taken from *Cook and Metzger* [1964], *McDaniel* [1964], and *Henry* [1967]. For O_2 the absorption cross section is seen to vary smoothly with wavelength except for significant changes in the vicinity of the O II(797) and O II(719) transitions. The atomic oxygen photo-ionization cross section is also structured in the vicinity of these two emissions [*Henry*, 1967]. Inspection of the measured ratios in Table 2 shows no pressure dependence for the O II(797)/O II(719) ratio, strongly suggesting that absorption by background O_2 and O at these wavelengths remained small under the operating conditions of this work. Since the absorption cross sections are smoothly varying function at the other wavelengths of interest, and since no pressure variation in the measured ratios was observed, it was concluded that pure absorption was small and did not significantly affect the results.

Discussion

Table 1 lists the calculated and observed intensity ratios for the multiplets and the corresponding branching ratios. The differences range from about 40% for r(555)/(601) to less than 10% for r(617)/(673), which is comparable to the systematic errors for the experiment estimated at 20%.

Dayglow observations of O II emissions were reported by *Gentieu et al.* [1979] and discussed in detail by *Feldman et al.* [this issue]. The ratios of the ^2D and ^2P emissions measured in the dayglow and listed in Table 1 are comparable to the laboratory values. All of the rocket ratios except r(578/581) are somewhat smaller than the laboratory results, and the differences are not inconsistent with the combined error limits of the two sets of data.

The rocket measurement of r(538/581) is very uncertain due to the unresolved overlay of the O II (538) by O II(539). The ratio of horizontal to upward viewing of the (538/539) emission feature and the weakness of the branching transition at O II(581) argues strongly that the O II(539) multiplet is dominant in the dayglow spectra.

The dayglow emissions terminating on the metastable O II levels are not expected to be strongly affected by resonance scattering because of the small optical thickness of the atmosphere. This is evident from Table 4, which gives values of σ_o, the line center scattering cross section, based on the calculated transition probabilities shown in Table 1. Using the analysis of *Torr et al.* [1979] that show the $O^+(^2D)$ and $O^+(^2P)$ densities are less than about 10^{-2} and 10^{-4} of the $O^+(^4S)$ density in the thermosphere, and using a typical mid-latitude total electron content of 1.0×10^{13} cm^{-2} [*Davies et al.*, 1975], the line center optical depths have been calculated and listed in Table 4. These upper limits to the optical depth are very much less than unity for the (555)/(601) and (617)/(673) pairs, and the $O^+(^2D)$ concentration would have to be greatly enhanced to be of any significance; however, for the (718)/(797) and (538)/(581) multiplets there are situations, such as during periods of high solar activity and in a limb viewing geometry, where multiple scattering will be important to the $^2D^0$ transitions.

Pure absorption by O, N_2, and O_2 will affect the observed atmospheric intensities especially now during solar maximum conditions. This is illustrated in Figure 5, where the absorption optical depths in the vertical and horizontal are plotted for a representative emission, i.e., $\lambda = 673$ Å. The integrated absorption coefficient is given by $\mu = \sigma_o [N] H \text{ Ch } (x, \chi)$, where σ_o is the absorption cross section given in Table 3, $[N]$ the number density of the absorbing species at the reference altitude h_o and scale height H for the MSIS model, and $T_\infty = 1376$ K. Values of the Chapman function (Ch) were taken from *Wilkes* [1953] for $\chi = 0$ and 90° appropriate for vertical and horizontal viewing geometries.

The principal absorbing species at 673 Å is molecular nitrogen, but for some of the shorter wavelength emissions absorption in atomic oxygen is dominant at the higher altitudes. Particular care is required for interpretation of dayglow measurements of r(797/718) ratio because of the large difference in the absorption cross sections for these two emissions.

CONCLUSIONS

These measurements of the lowest of the O II (^2D) and (^2P) branching ratios have been carried out using two types of sources and at various pressures and lamp current conditions, and the results are insensitive to any of these parameters. We thereby conclude that resonance and pure absorption in the source region is not important and no strong source dependent factors are operative.

The agreement with theoretical values and dayglow observations is very good considering the experimental uncertainties and the theoretical difficulties in the calculation of the transition probabilities.

REFERENCES

Christensen, A. B., A rocket measurement of the extreme ultraviolet dayglow, *Geophys. Res. Lett. 3*, 221–224, 1976.

Cohen, M., and A. Dalgarno, An expansion method for calculating atomic properties, IV, Transition probabilities, *Proc. Roy. Soc., Ser. A, 280*, 258–270, 1964.

Cook, G. R., and P. H. Metzger, Photoionization and absorption cross sections of O_2 and N_2 in the 600- to 1000-Å region, *J. Chem. Phys., 41*, 321–336, 1964.

Davies, K., R. B. Fritz, R. N. Grubb, and J. E. Jones, Some early results from the ATS-6 radio beacon experiment, *Radio Sci. 10*, 785–799, 1975.

Feldman, P. D., D. E. Anderson, Jr., R. R. Meier, and E. P. Gentieu, The ultraviolet dayglow, 4: The spectrum and excitation of singly ionized oxygen, *J. Geophys. Res.*, this issue.

Gentieu, E. P., P. D. Feldman, and R. R. Meier, Spectroscopy of the extreme ultraviolet dayglow at 6.5 Åresolution: atomic and ionic emissions between 530 and 1240 Å, *Geophys. Res. Lett., 6*, 325–328, 1979.

Henry, R. J. W., Photoionization cross sections for atomic oxygen, *Planet. Spac Sci., 15*, 1747–1755, 1967.

Kelly, P. S., Som analytical self-consistent field functions and dipole transition matrix elements for nitrogen and oxygen and their ions, *Astrophys., J., 140*, 1247–1268, 1964.

Luken, W. L., and O. Sinanoglu, Oscillator strengths for transitions involving excited states not lowest of their symmetry oxygen I and oxygen II transitions, *J. Chem. Phys., 64*, 1495–1497, 1976.

McDaniel, E. W., *Collision Phenomena in Ionized Gases*, p. 351, John Wiley, New York, 1964.

Paresce, F., S. Kumar, and C. S. Bowyer, A continuous discharge line source for the extreme ultraviolet, *Appl Opt., 10*, 1904, 1971.

Torr, D. G., K. Donahue, D. W. Rusch, M. R. Torr, A. O. Nier, D. Kayser, W. B. Hanson, and J. H. Hoffman, Charge exchange of metastable ^2D oxygen ions with molecular oxygen: A new source of thermospheric O_2^+ ions, *J. Geophys. Res., 84*, 387–392, 1979.

Wiese, W. L., M. W. Smith, and B. M. Glennon, *Atomic Transition Probabilities*, vol. I, *Hydrogen Through Neon, Nat. Stand. Ref. Data Ser. 4*, National Bureau of Standards, Washington, D. C., 1966

Wilkes, M. V., a Table of Chapman's grazing incidence integral, *J. Phys. B, 67*, 304–308, 1954.

(Received August 14, 1980;
revised November 24, 1980;
accepted November 26, 1980.)

Paper number 80A1737.
0148-0227/81/080A-1737$01.00

Fig. 1. Term diagram for O II. Solid lines indicate observed atmospheric transition. Dashed lines are dipole forbidden intersystem transitions.

Fig. 2. Schematic diagram showing the layout of optical components. Extreme ultraviolet radiation generated in the discharge source was dispersed in the windowless Seya-Namioka monochromator and detected by a spiral electron multiplier.

Fig. 3. Low-resolution spectrum observed with the hollow cathode discharge source showing the O I and O II emissions in the 500- to 840-Å region. Intensities are raw uncorrected output currents.

Fig. 4. High-resolution spectra of the principle O II multiplets. Intensities are uncorrected for detector sensitivity. Sensitivity was reduced by a factor of 6 while recording the 718, 797, and 834 multiplets.

Fig. 5. Vertically and horizontally integrated total absorption at 673 Å for a MSIS model atmosphere with T_∞ = 1376°K. Absorption cross sections were 2.3×10^{-17} cm^2, 2.5×10^{-17} cm^2, and 0.6×10^{-17} cm^2 for N_2, O_2, and O, respectively.

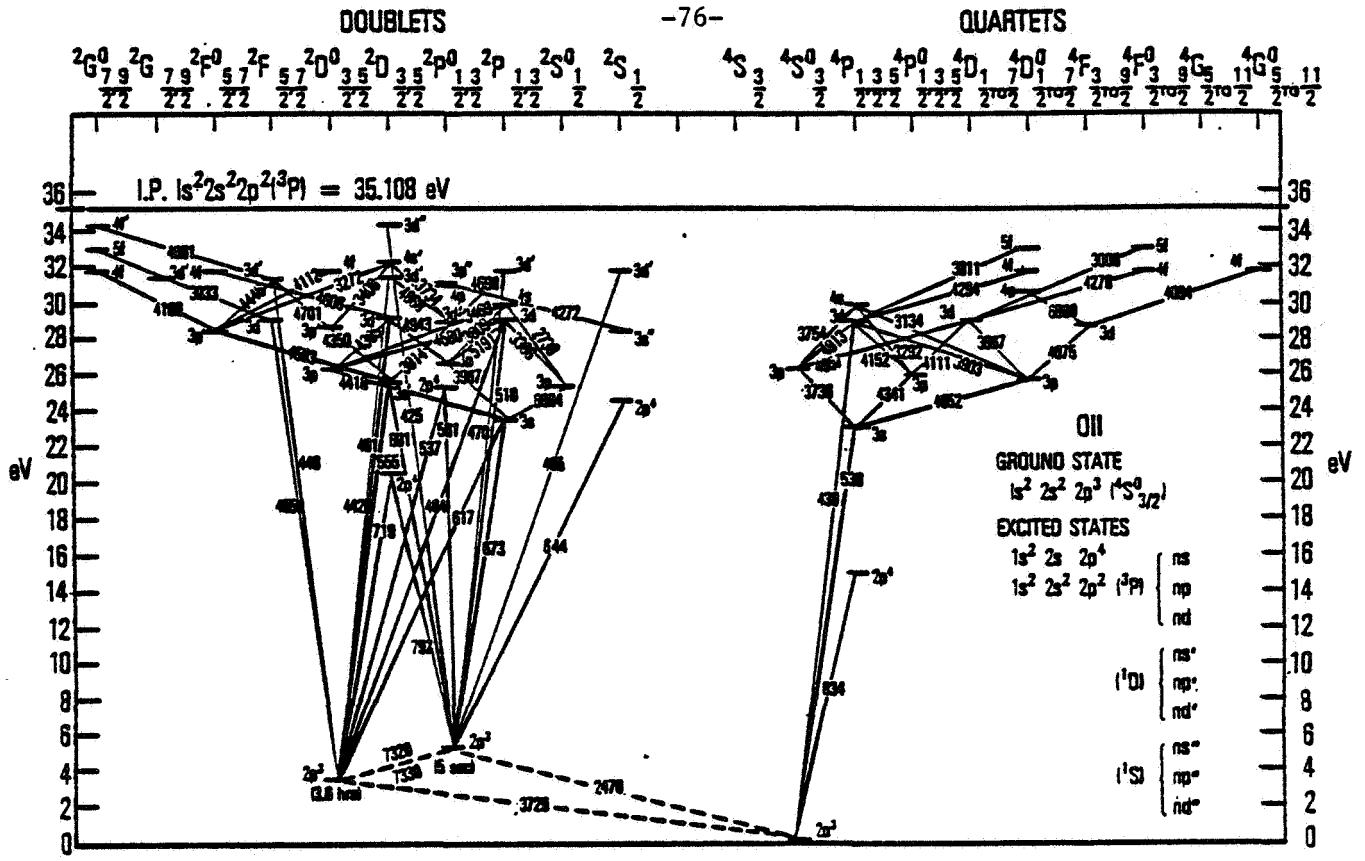

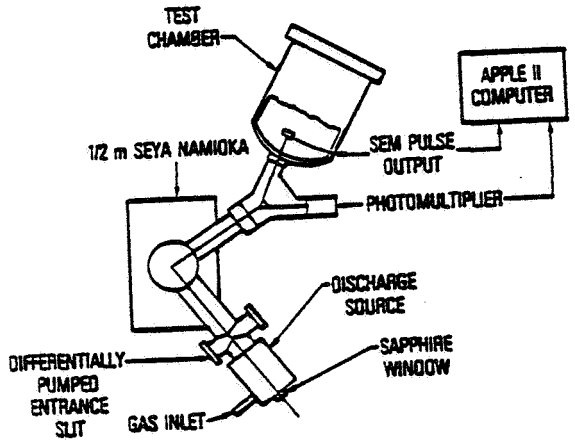

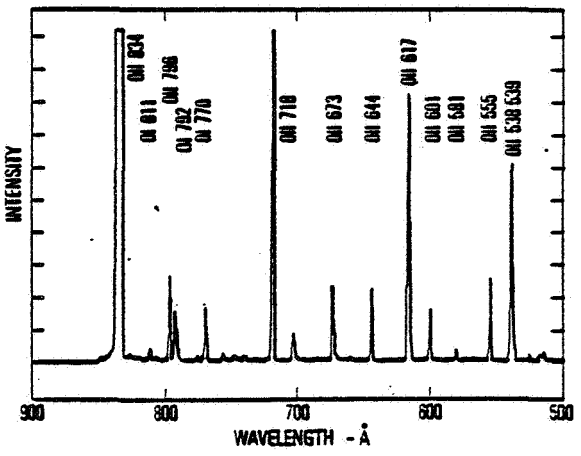

AGU SOA1757
- Morrison et al.
- 2
50%

AGU SOA1757
- Morrison et al.
- 3
50%

Multiplet	N_2	O_2	O.	Comments
797	2.8	3.5	0.3	much structure in N_2
718	2.5	3.1	0.6	some structure in O_2
673	2.3	2.5	0.6	
617	2.9	2.5	0.9	
601	2.9	2.0	0.9	
555	1.8	2.0	1.0	
581	2.1	2.0	1.0	
537	1.4	2.0	1.0	

From *Cook and Metzger* [1964], *McDaniel* [1964], and *Henry* [1967]. Units are 10^{-17} cm^2.

TABLE 4. Line Center Scattering Cross Section at 800°K and Atmospheric Vertical Optical Depth for $O^+(^2D)$ at 1×10^{11} cm^2 and $O^+(^2P)$ at 1×10^9 cm^2

Term	Wavelength	g	S	σ_0* cm^2	τ (Vertical)
$^2D^0$–^2D	718	10	6	3×10^{-13}	3×10^{-2}
$^2P^0$–^2D	797	6	1.3	1×10^{-13}	1×10^{-4}
$^2D^0$–^2D	555	10	1.2	6×10^{-14}	6×10^{-3}
$^2P^0$–^2D	601	6	0.5	4×10^{-14}	4×10^{-5}
$^2D^0$–^2P	617	10	1.2	6×10^{-14}	6×10^{-3}
$^2P^0$–^2P	673	6	0.8	7×10^{-14}	7×10^{-5}
$^2D^0$–^2P	538	10	6.0	3×10^{-13}	3×10^{-2}
$^2P^0$–^2P	581	6	2.3	2×10^{-13}	2×10^{-4}

*$\sigma_0 = 8.06 \times 10^{-6}\, S/g = (2\pi kT/M)^{1/2}$.

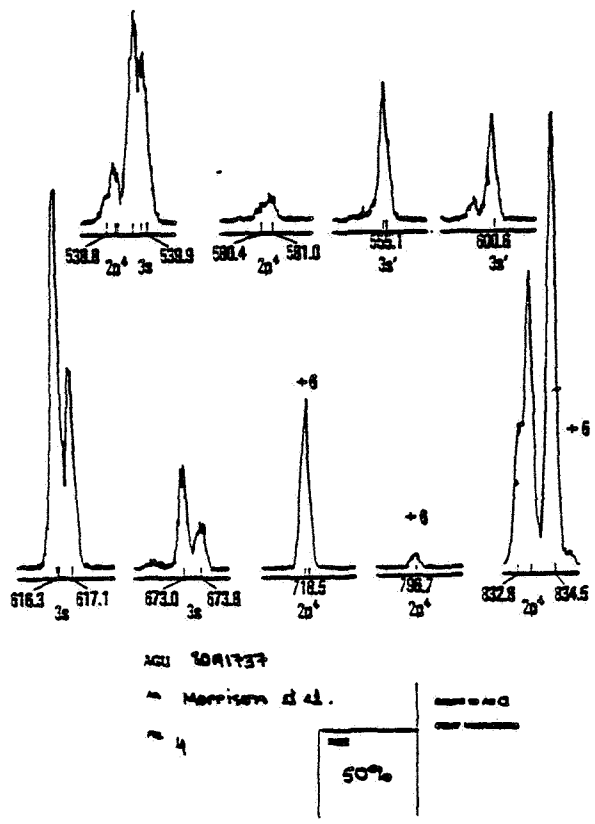

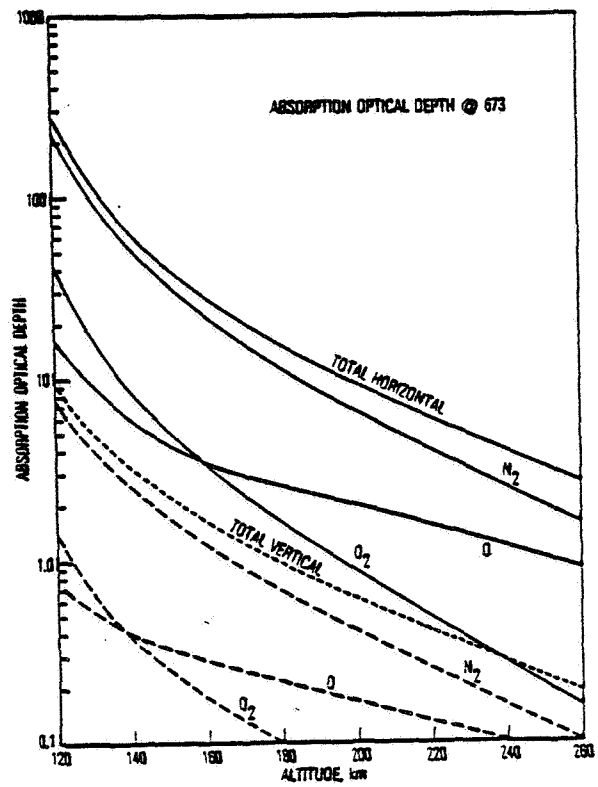

TABLE 1. Calculated and Measured Branching and Intensity Ratios for O II Transitions

Configuration	Term	Wavelength, Å	A*		B		C		D† (r)	Present Measurements	
			r	ω̄	r	ω̄	r	ω̄		r	ω̄
$2s^22p^3$–$2s2p^4$	$^2D^0$–^{2}	718		0.88		0.86					0.91
			7.3		6.4				5.9 ± 3.0	9.7 ± 0.9	
$2s^22p^3$–$2s2p^4$	$^2P^0$–^2D	797		0.12		0.14					0.09
$2s^22p^3$–$2s^22p^2(^1D)3s'$	$^2D^0$–^2D	555		0.78							0.69
			3.5						1.0 ± 0.05	2.2 ± 0.2	
$2s^22p^3$–$2s^22p^2(^1D)3s'$	$^2P^0$–^2D	601		0.22							0.31
$2s^22p^3$–$2s^22p^2(^3P)3s$	$^2D^0$–^2P	617		0.66				0.86			0.85
			2.0				5.9		3.6 ± 1.1	5.5 ± 0.5	
$2s^22p^3$–$2s^22p^2(^3P)3s$	$^2P^0$–^2P	673		0.34				0.14			0.15
$2s^22p^3$–$2s2p^4$	$^2D^0$–^2P	538				0.77		0.77			0.72
					3.3		3.3		>5.5	2.6 ± 0.4	
$2s^22p^3$–$2s2p^4$	$^2P^0$–^2P	581				0.23		0.23			0.28

Columns are A, *Wiese et al.* [1966]; B, *Cohen and Dalgarno* [1964]; C, *Luken and Sinanoglu* [1976]; D, *Feldman et al.* [this issue].
*Theoretical.
†Dayglow observation.

TABLE 2. Measured Intensity Ratio at Various Source Pressures

Multiplets	32* at 500 ma	33* at 500 ma	40 at 300 ma	65 at 400 ma	150 at 465 ma	Average
Hollow Cathode Source						
718/796			9.8	9.3	10.4	9.8 ± 0.6
555/601			2.4	2.2	2.4	2.3 ± 0.1
617/673			5.6	6.1	5.0	5.6 ± 0.5
538/581	2.9	2.7				2.8 ± 0.1
539/617			2.0	2.0	2.0	...
834/617			5.6	5.2	9.2	...

Multiplets	28 at 365 ma	28 at 500 ma	32 at 450 ma	34 at 450 ma	34 at 450 ma	37* at 180 ma	70 at 450 ma	85 at 300 ma	Average
Capillary Discharge Source									
718/797	9.0	10.0	9.0	10.6	10.7		8.4	10.0	9.7 ± 0.9
555/601	2.1	2.1	2.2	1.6	2.2	2.4	2.2	2.1	2.1 ± 0.2
617/673	5.3	5.9	5.1	5.1	4.4	6.1	6.1	5.5	5.4 ± 0.6
538/581						2.8		2.2†	2.5 ± 0.4

O_2 pressure is in microns of mercury.
*Apple computer runs.

ELECTRIC COUPLING OF THE E AND F REGIONS

R.A. Heelis

Since the renewed interest in the effects of electrical coupling between the E and F regions (Fejer et al., 1979) we have successfully implemented the computational techniques employed by Heelis et al. (1974) to model these effects on the UTD Space Sciences computer. Computations are carried out in two phases. First a solution for the electrostatic potential distribution in the E-region is obtained using a model for the E region conductivity distribution and for the dynamo neutral wind field. In these calculations the E-region is assumed to be a thin slab and the diurnal variation of conductivity is proportioned to the ion concentration in the slab, which is shown in Figure 1. The variation of conductivity with latitude is assumed to change like the cosine of the solar zenith angle. The solar diurnal tidal wind is thought to be the dominant wind field producing the equatorial Sq current system (Tarpley, 1970) and the electrostatic potential obtained from this wind system is shown in Figure 2. This potential distribution is mapped along the magnetic field lines into the F-region where the second phase of the calculations are implemented. We first calculate the vertical drift and the east-west drift of the plasma in response to the applied electric field. Results of these calculations are shown in Figure 3. Also shown are similar results when a solar semi-diurnal tide is included in the E-region. These results are very similar to those obtained by Heelis et al. (1974) and we now plan to pursue two new directions while assembling the data for publication.

First, we plan to determine the effects of changing the diurnal variation of the E-region conductivity. If it is evident that the reversal in the F-region drift velocity occurs about 2 or 3 hours before that observed by ground based radar

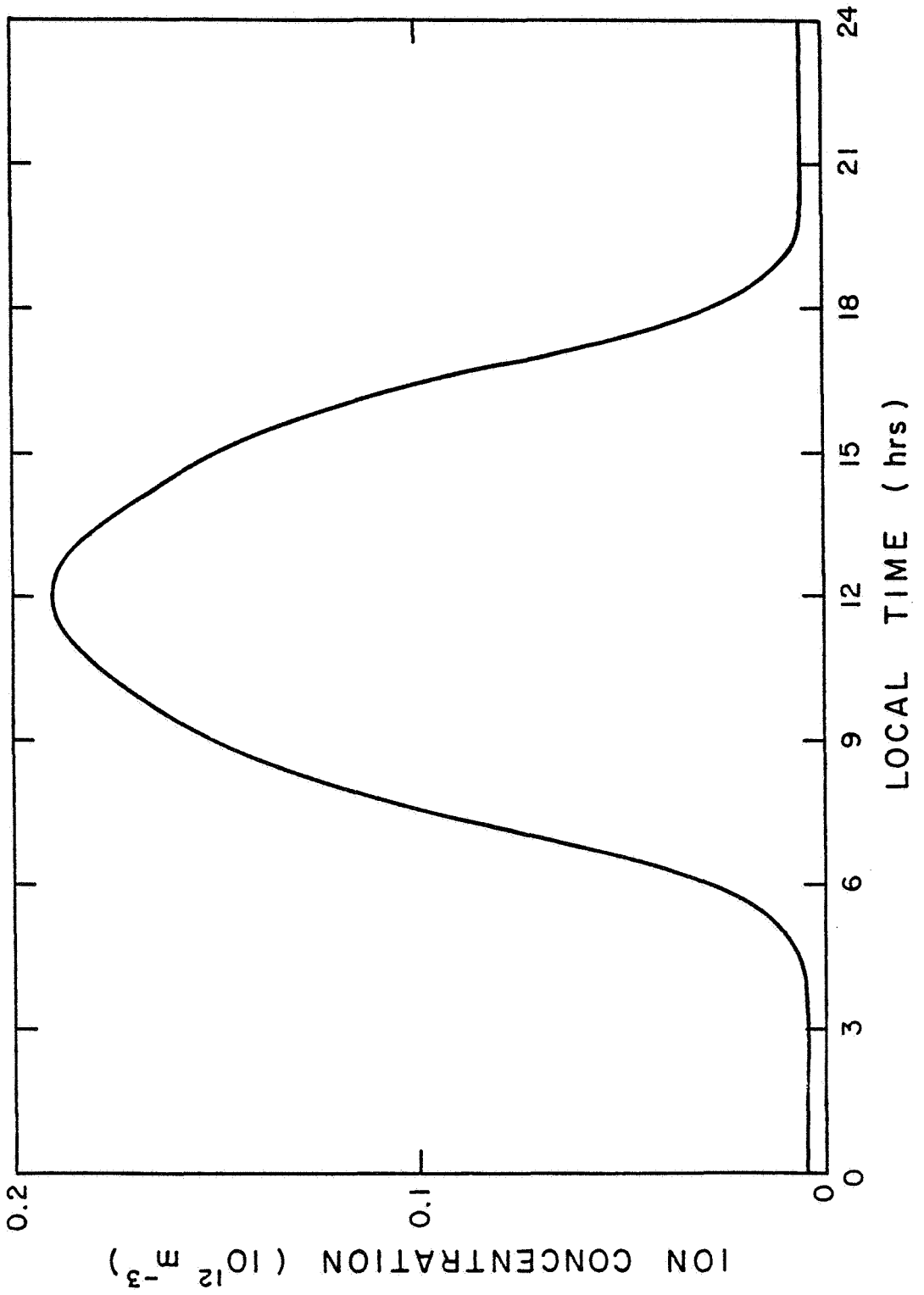
ION CONCENTRATION (10^{12} m^{-3})
0.2
0.1
0
0
3
6
9
12
15
18
21
24
LOCAL TIME (hrs)

FIGURE 1

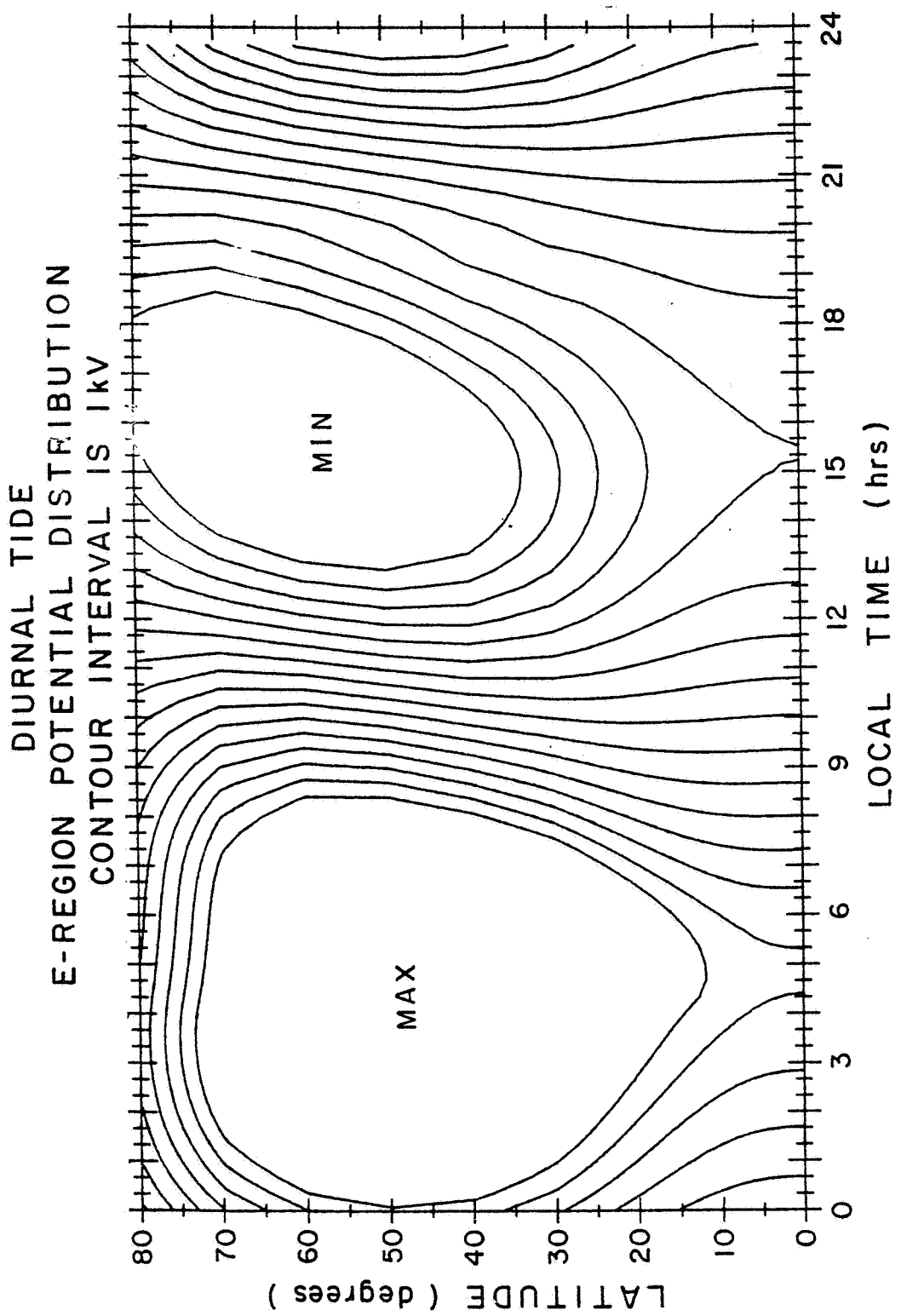
DIURNAL TIDE
E-REGION POTENTIAL DISTRIBUTION
CONTOUR INTERVAL IS 1kV
MAX
MIN
LATITUDE (degrees)
80
70
60
50
40
30
20
10
0
0
3
6
9
12
15
18
21
24
LOCAL TIME (hrs)

FIGURE 2

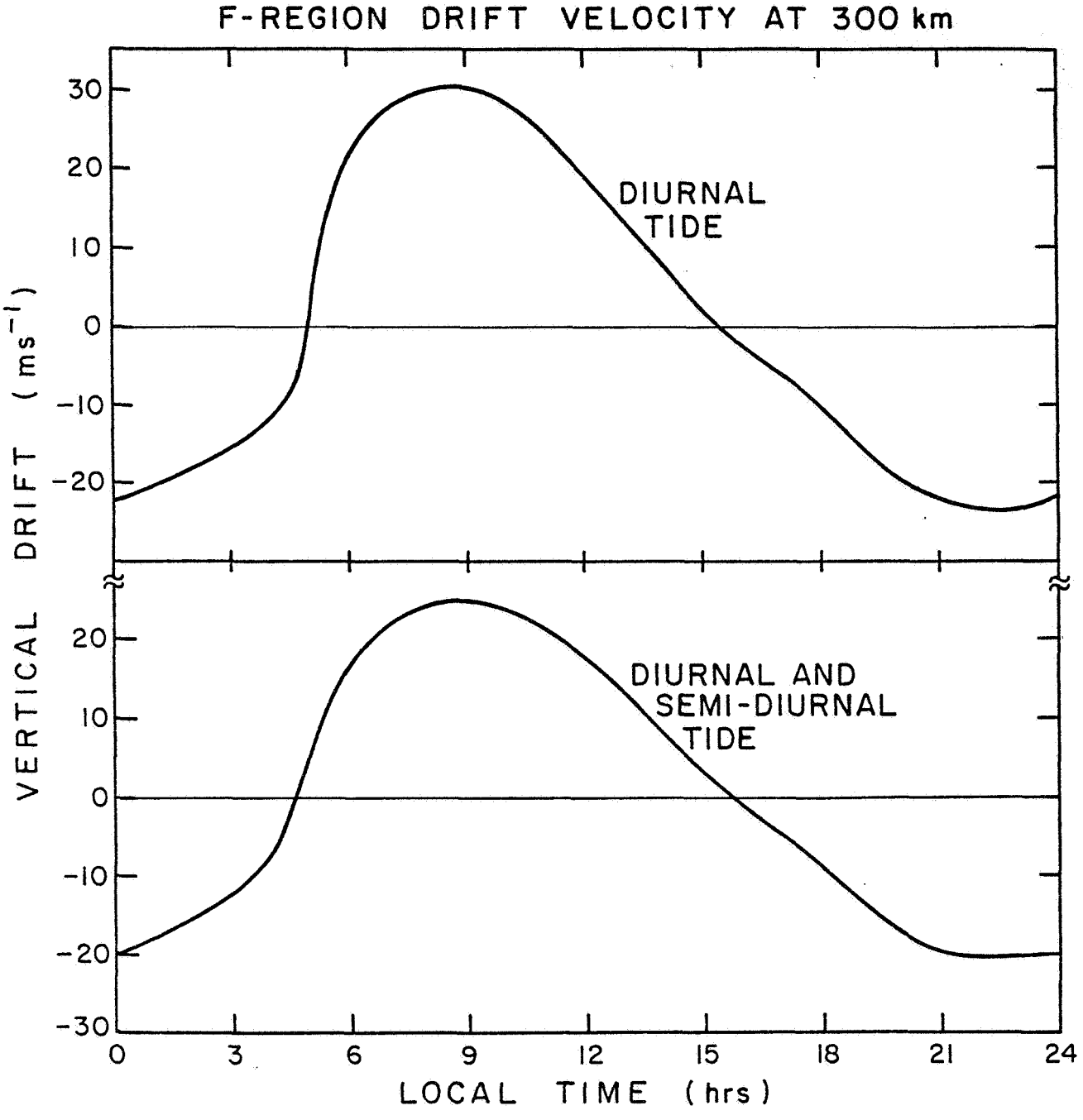
F-REGION DRIFT VELOCITY AT 300 km
VERTICAL DRIFT (ms⁻¹)
30
20
10
0
-10
-20
DIURNAL TIDE
20
10
0
-10
-20
-30
DIURNAL AND SEMI-DIURNAL TIDE
0
3
6
9
12
15
18
21
24
LOCAL TIME (hrs)

FIGURE 3

It appears prudent therefore to investigate the effects of extending the daytime E-region ion concentrations a little beyond 18:00 hours. Secondly we plan to investigate the effects of F-region neutral wind fields and their phase with respect to the E-region conductivity. We expect to learn more about the mechanism that produces enhanced upward velocities near 18:00 hours from this study.

References:

Fejer, B.G., D.T. Farley, R.F. Woodman and C. Calderon, Dependence of Equatorial F-Region Vertical Drifts on Sensor and Solar Cycle, J. Geophys. Res., 84, 5792, 1979.

Heelis, R.A., P.C. Kendall, R.J. Moffett, D.W. Windle and H. Rishbeth, Electrical Coupling of the E and F Regions and its Effects on F Region Drifts and Winds, Planet. Space Sci., 22, 743, 1974.

Tarpley, J.D., The Ionospheric Wind Dynamo, 2, Solar Tides, Planet. Space Sci., 18, 1091, 1970.

Dy

SPACE SCIENCE COMPUTATIONAL ASSISTANCE

R.C. Chaney

The PDP 11/45 continues to provide significant support to the computational aspects of the space science research at The University of Texas at Dallas. Dr. Hoffman continues to use the machine for analysis of data from the ion mass spectrometer on the ISIS-2 satellite. Dr. Klumpar continues to use the machine for ISIS sounding rocket data analysis and plotting. Dr. Heelis is using the 11/45 for three separate activities: 1) The study of the electrical coupling in the E and F regions of the ionosphere; 2) The development of a model of the ionospheric convection pattern in terms of analytical functions and; 3) Limited interactive data analysis from the Dynamics Explorer mission. Dr. Coley is using the machine for reduction and analysis of Atmospheric Explorer-C magnetometer data for the purpose of detection of field aligned currents in the upper atmosphere at high latitudes. Dr. Rohrbaugh is using the machine to perform modeling of the atomic hydrogen distribution in the terrestrial exosphere using Monte-Carlo techniques. Data analysis for the San Marco Ion Velocity Instrument, built here at The University of Texas at Dallas will be done on the PDP 11/45. We have a computer link between the PDP 11/45 and the PDP 11/23 for transfers of Dynamics Explorer data between the two machines. The machine continues to be a cost effective, convenient and reliable tool for computational work in space sciences.

SPACE SCIENCE SEMINAR PROGRAM

J.P. McClure

The seminar series has remained an important part of the Space Science program at The University of Texas at Dallas. The faculty, students, and staff regularly present seminars on their specialties, and in addition we invite outside speakers to present seminars on special topics. These speakers are usually leading atmospheric or magnetospheric scientists and/or collaborators with us on various scientific projects. We find that having these visitors in Dallas is very stimulating and productive.

The following seminars and lectures were presented during this reporting period.

Dr. William Knudsen, Lockheed Palo Alto Research Laboratory, "The Ionosphere of Venus", October 22, 1980.

Dr. Chris Goertz, University of Iowa, "Parallel Electric Fields and Alfven Waves", October 27, 1980.

Dr. Thomas Donahue, University of Michigan, "Volatiles in the Atmosphere of Venus and their Implications for the Origins of the Terrestrial Planets", October 30, 1980.

Dr. Colin Hines, University of Toronto, "Atmospheric Gravity Waves", November 3, 1980.

Dr. A.J. Dessler, Rice University, "Jupiter as a Pulsar: The Magnetic Anomaly Model", December 2, 1980.

Dr. J. Patrick Lestrade, Texas A & M University, "Light Scattering in Planetary Atmospheres", December 5, 1980.

Dr. Sandy Murphree, University of Calgary, "Two Dimensional Imaging of the Aurora: The Importance of Interpreting Observations from the Magnetospheric Point of View", December 16, 1980.

Dr. Eldon Ferguson, Aeronomy Laboratory — NOAA, "Stratospheric Ion Chemistry", March 6, 1981.

Dr. Larry Lyons, NOAA, "Auroral Electrodynamics", February 18, 1981.

Dr. Konrad Mauersberger, University of Minnesota, "The Neutral Atmosphere Between 20 and 40 km", April 24, 1981.

Dr. Wesley T. Huntress, Jet Propulsion Labs, Pasadena, California, "Upper Atmospheric Research Programs at JPL", May 6, 1981.

VISITING SCIENTIST PROGRAM

W.B. Hanson

Considerable scientific progress, cross fertilization and a broadening of our science base at UTD has been realized this year from visits by two scientists from outside institutions.

Dr. L.R. Lyons from the National Oceanographic and Atmospheric Administration in Boulder, Colorado was able to visit UTD in the past six months to discuss some aspects of ionosphere-magnetosphere coupling of mutual interest. At UTD we have begun development of an analytical model that describes the convective flow of plasma in the F-region. We are attempting to make this model, based on an electrostatic potential distribution, as realistic as possible. That is we wish to be able to reproduce a realistic pattern of field aligned currents and auroral arcs. Dr. Lyons has recently developed a model that self-consistently calculates the field aligned currents and auroral arc structure from a given magnetospheric potential distribution. The exchange of ideas and information that took place regarding our research objectives was extremely valuable. We were able to acquire the appropriate computer code for Dr. Lyons' model and anticipate further use and future interaction with him in this area.

Dr. Sandy Murphree of the University of Calgary consulted with members of the Center scientific staff from the 15th to the 19th of December, 1980. Dr. Murphree's area of expertise, the optical imaging of the auroral oval from space, is highly complementary to our own research efforts that concentrate on the electrodynamic coupling and the charged particle input to the auroral regions. During his visit, Dr. Murphree brought to UTD the complete

set of auroral images in 5577Å and 3914Å taken during the operation of the ISIS-2 satellite. Intensive review and discussion of this large data set during his visit provided further insight for our auroral oval studies and stimulated collaborative work on the particle acceleration processes during substorms. During his visit Dr. Murphree also presented a seminar entitled, Two-Dimensional Imaging of the Aurora: The Importance of Interpreting Observations from the Magnetospheric Point of View".

WAVE INSTABILITIES IN INHOMOGENEOUS PLASMAS

B.L. Cragin

The extension to three dimensions of the one-dimensional calculations described in our last Semi-Annual report has been completed, and considerable progress has been made in the physical interpretation of these results. It is now believed that a quite convincing case can be made that a description of nonlinear Landau damping in terms of the global normal modes of the plasma does indeed remain meaningful even if the spatial extent of these modes (or the plasma inhomogeneity scale length) is large compared with the distance that a packet of electron plasma waves can travel in a typical nonlinear interaction time scale.

One of the central questions at issue, of course, was the interplay between local and global concepts in plasma turbulence theory. Somewhat similar considerations have been the source of much debate in the field of quantum mechanics. Thus it is perhaps not too surprising that the quantum-mechanical interpretation of nonlinear Landau damping - a viewpoint pioneered by Tsytovich, Goldman and Dubois, Hasegawa and others - turned out to be of interest in this context.

One of the most significant points to come out of this work concerns the relationship between the classical normal modes of the plasma wave field and the quantum-mechanical stationary states of the field quanta. These quanta, known as plasmons, correspond to the longitudal (zero-spin) state of the photon. The effective mass of a plasmon can be calculated from the characteristic range of the plasmon propogator, as in quantum field theory, or (in the WKB limit) from the inertial mass of a localized single-plasmon wave packet.

The fact that plasmons have integer spin and are hence bosons implies that an arbitrarily large number of them can occupy the same quantum-mechanical state. In the classical limit of large "occupation numbers" a close correspondence is found between the classical normal modes and the quantum wave functions of the underlying stationary states. In the quantum-mechanical treatment of nonlinear Landau damping, the process is viewed as resulting from induced transitions between states of differing momentum and energy. Thus, the coupling coefficients between modes in the classical global-interaction description can be given a new, essentially quantal, interpretation in terms of the induced transition probability per unit time.

The fact that classical calculations of this kind sometimes turn out to give quantum-mechanically correct results is of course nothing new, since other examples of this have been found (the free-electron laser is an example). What does seem to be new is the realization that when this occurs in problems involving finite boundaries or spatial inhomogeneity, so that the classical normal modes of the system (and also the quantum eigenstates) are no longer of the plane-wave form, a paradox seems to arise concerning the rate at which energy or information is transmitted through space. In this way we have been able to show that the paradox that originally motivated this investigation is, in fact, rather closely related to the famous EPR (Einstein-Pololsky-Rosen) paradox of quantum theory. The results of recent laboratory experiments tend to support the view that it is safest to take a global point of view from the start and not to be too disturbed about the apparent breakdown of the locality suggested by causal considerations.